Journal of Achievements in Materials and Manufacturing Engineering
VOLUME 31
ISSUE 2
December
2008

Mechanical properties of Co-based amorphous ribbons

J. Konieczny [a], L.A. Dobrzański [a,*], L. Pešek [b], P. Zubko [b]
[a] Division of Materials Processing Technology, Management and Computer Techniques in Materials Science, Institute of Engineering Materials and Biomaterials, Silesian University of Technology, ul. Konarskiego 18a, 44-100 Gliwice, Poland
[b] Department of Materials Science, Technical University of Košice, Park Komenkeho 12, 042 00 Košice, Slovakia
* Corresponding author: E-mail address: leszek.dobrzanski@polsl.pl

Received 12.09.2008; published in revised form 01.12.2008

Materials

ABSTRACT

Purpose: The goal of this work was to investigate the influence of chemical composition and isothermal heating in order to determine the change of the mechanical properties of the metallic ribbons by depth sensing indentation technique.
Design/methodology/approach: The amorphous metallic ribbons were manufactured by planar-flow-casting method. Instrumented hardness measuring was carried out using the nanohardness tester DUH-202 with a Vickers indenter. Observations of the structure of powders were made on the OPTON DSM-940 scanning electron microscope. The diffraction examinations and examinations of thin foils were made on the JEOL JEM 3010 transmission electron microscope.
Findings: The analysis of the mechanical properties and structure of the Co-based amorphous ribbons obtained in the by planar-flow-casting process proved that the no significant differences between both ternary alloys in local mechanical properties HM, EIT and W were observed for amorphous state but differences between ternary and multicomponent alloys were observed. In heat treated state small differences between materials were observed too.
Research limitations/implications: For the metallic Co-based amorphous ribbons, further mechanical examinations and structure are planed.
Practical implications: Feature an alternative to commercial alloys and composite materials are the amorphous and nanocrystalline metal amorphous ribbons obtained by melt spinning technique and make it possible to obtain the new composite materials with best mechanical properties, whose dimensions and shape can be freely formed.
Originality/value: The paper presents influence of annealing temperature and chemical composition of metallic ribbons on martens hardness, indentation modulus EIT, work for deformation and ratio of elastic and total indentation energy. Heating of ribbons obtained by melt spinning technique, to check its effect on changes of mechanical properties. Results and a discussion of the influence of annealing temperature microhardness metallic ribbons is presented.
Keywords: Amorphous materials; Mechanical properties; Electron microscopy; Heat treatment

1. Introduction

The metallic amorphous and nanocrystalline alloys are characterisitic for their very good mechanical properties which are different from their classic equivalents [3, 6, 16]. The early results of the mechanical properties and hardness tests of the nanocrystalline materials revealed that their significant strengthening (hardening) may be obtained by decreasing their grain size from the macro- range, through micro- to the

nanometric scale [13]. Observations on the electron transmission microscope have revealed that the isolated clusters and grains of the nanocrystalline materials do not contain dislocations Metal materials with the nanocrystalline structure, free from numerous dislocations capable of relocating, are much stronger than their classic equivalents [19, 21].

By reason of increased anticorrosive properties [20] and high mechanical properties [7, 22] the magnetic amorphous and nanocrystalline materials [9, 11, 18] are also very interesting for scientists. Fast cooled alloys (ribbons) with Co matrix are characteristic for their ultimate tensile strength UTS exceeding 1200 MPa, Young modulus 80 GPa and microhardness between 360-380 DPN (*diamond pyramid number* 1 DPN =1kg/mm^2 = 9,8 MPa) [5, 12].

DSI technique is based on continuous measuring (instrumented hardness measuring) of applied indentation force, F, in dependence on indentation depth, h, during hardness measuring, so that an indentation curve, F–h (Fig 1), can be determined. The method was introduced in 1992 for measuring hardness and elastic modulus. Instrumented indentation technique has widely been used in the characterization of mechanical behaviour of materials at small scales [14, 15, 17]. Because of very small indents, which are not measurable optically with appropriate accuracy, the hardness is calculated from h on the basis of known indenter geometry. Several parameters may be derived from the indentation curve.

According to Oliver and Pharr [14] the relationships between penetration depth (h) and load (F) for such indenter geometries can be represented in the form:

$$F = \alpha(h - h_f)^m \tag{1}$$

where: α – is empirical constant determined after unloading data fitting, h – is the elastic displacement, h_f – is the final unloading depth, and m – is a power law exponent that is related to the geometry of the indenter (for a flat-ended cylindrical punch, m = 1, for a paraboloid of revolution, m = 1.5, and for a cone, m = 2).

Martens hardness [1] is defined for every point of the indentation curve (pair of values F and h) as:

$$HM = \frac{F}{A_s(h)} = \frac{F}{kh^2} \tag{2}$$

F [N] – actual loading force, k = 26,43 for Vickers [1] indenter and 26,44 for Berkovich [10], h – corresponding indentation depth during loading. The results on indentation curve, Fig. 3. Martens hardness HM is measured under applied load, so that both plastic and elastic deformation are taken into consideration (Fig. 1a). Moreover, the elastic unloading depends on the modulus of elasticity E, therefore it can be measured by this way. Additionally, the work done during indentation may be used to characterize the ability of the material to absorb the plastic, W_{plast}, and elastic, W_{elast}, energy (Fig. 1b).

The area below the part of the indentation curve F-h corresponds to the energy for the total indentation deformation W, the area below the unloading part to the energy of elastic deformation W_{elast}. The difference gives the plastic deformation energy [2]:

$$W_{plast}=W_{total} - W_{elast} \tag{3}$$

In "classic" Vickers microhardness testing, the hardness value is determined by measuring the diagonal of the resulting unrecovered indentation using a microscope.

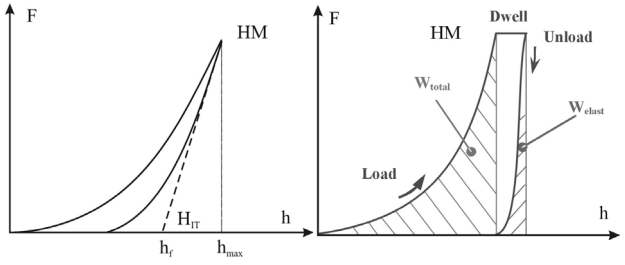

Fig. 1. Indentation curve a), indentation energy W: total, elastic and plastic b)

The vertical displacement of the contact periphery [14], it follows from the geometry of that depth along which contact is made between intender and the specimen $h_c = h_{max} - h_s$ is (Fig. 2):

$$h_c = h_{max} - \varepsilon \frac{F_{max}}{S} \tag{4}$$

ε=0.72 for a conical punch, ε=0.75 for a paraboloid of revolution (which approximates to a sphere at small depths), and ε=1.00 for a flat punch, S – elastic unloading stiffness:

$$S = \frac{dF}{dh} \tag{5}$$

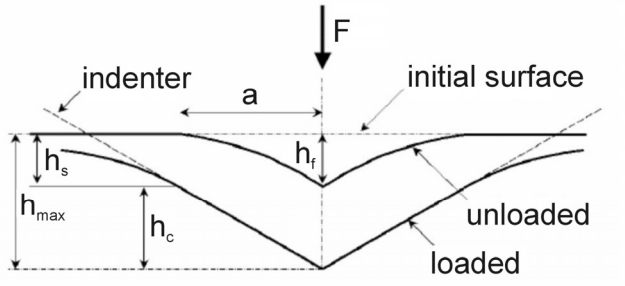

Fig. 2. Schematic illustration of the unloading process showing parameters characterizing the contact geometry; F – test force, h_{max} – maximum indentation depth at F_{max}, h_c – depth of the contact of the intender with the test piece at F_{max}, h_s – permanent indentation depth after removal of the test force (deflection), h_f – depth of the contact [14]

The deflection of the surface at the contact is:

$$h_s = \left(\frac{\pi - 2}{\pi}\right)\left(h - h_f\right) \tag{6}$$

Because the Vickers indenter tip is not perfect, h_{max} is replaced by a corrected depth, h_{corr}, in a depth function of the form:

$$h_{corr} = \sqrt{h^2(1 + kh'')} \tag{7}$$

where h_{corr} corresponds to equivalent depths from an ideal Vickers indenter, and k and n are empirical parameters. The surface area of the indenter is determined through the expression:

$$A = 26{,}43h_{corr}^2 \tag{8}$$

Indentation hardness H_{IT} [N/mm^2] is [2]:

$$H_{IT} = \frac{F}{A_p} \tag{9}$$

where A_p - contact area at maximum load, with A_p=24,5*h_c for Vickers indenter and A_p=23,96*h_c for Berkovich indenter

$$h_c = h_{\max} - \frac{\varepsilon(h_{\max} - h_s)}{n} \tag{10}$$

where ε= 0.72 for a pyramid, and ε= 0.75 for a sphere for Vickers and Berkovich indenter, n – unloading index.

Indentation modulus E_{IT} [N/mm^2] can be estimated on the relationship basis) [2]:

$$E_{IT} = \frac{1 - v_s^2}{\frac{1}{E_r} - \frac{1 - v_i^2}{E_i}} \tag{12}$$

where E_r is reduced biaxial modulus [1]:

$$E_r = \beta \frac{\sqrt{\pi}}{2} \cdot \frac{S}{\sqrt{A_c}} \tag{13}$$

v – Poisson ratio, S – elastic unloading stiffness, i – indenter (diamond v=0.07, E=1140 GPa), β – corresponds to a correction factor related to the lack of symmetry of the indenter (equal to 1.0124 for Vickers indenters), A_c – is the projected contact area.

In this case the area is simply computed from the radius of the contact:

$$A_c = \pi a^2 \tag{14}$$

which is calculated from the following expression:

$$a = \sqrt{2h_c R - h_c^2} \tag{15}$$

where R is the nominal radius of the intender tip. Ratio of elastic and total indentation energy η can be estimated on the basis of following relationship [5]:

$$\eta_{IT} = \frac{W_{elast}}{W_{total}} \cdot 100\% \tag{16}$$

The goal of this work was to investigate the influence of chemical composition and isothermal heating in order to determine the change of the mechanical properties of the metallic ribbons by depth sensing indentation technique.

2. Experimental

Instrumented hardness measuring was carried out using the nanohardness tester DUH-202 (Shimadzu) with a Vickers indenter. The load used was 500 mN (≈50 g), after reaching it a 5 sec dwell time followed. Martens hardness HM, indentation modulus E_{IT} which correspond to the Young modulus (modulus of elasticity) and both total work for deformation W_{total} and elastic work W_{elast} (W_{plast}=W_{total}-W_{elast}) were determined from the indentation curve.

The hardness was measured in the plane perpendicular to the ribbon surface. Investigations were carried out of the specimens from the $Co_{77}Si_{11,5}B_{11,5}$, $Co_{68}Fe_4Mo_1Si_{13,5}B_{13,5}$ and $Fe_{79}Si_{13}B_9$ metallic glasses in the form of the 0.026 mm thick and 10.2 mm wide ribbons.

For the $Co_{77}Si_{11,5}B_{11,5}$ and $Co_{68}Fe_4Mo_1Si_{13,5}B_{13,5}$ alloys in the "as quenched" state and after their isothermal heat and for $Fe_{79}Si_{13}B_9$ after isothermal heating 10 indents were applied for each material; for $Fe_{79}Si_{13}B_9$ in the "as quenched" state 20 indents were applied. A significant scatter of the test values was observed for the $Fe_{79}Si_{13}B_9$ alloy in the "as quenched"; therefore, the number of measured values was increased. The regular indentation curves (Fig. 3) were inspected and irregular (Fig. 4) curves were excluded from the statistics (Table 1).

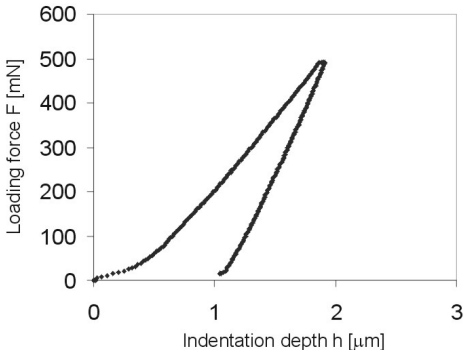

Fig. 3. Regular indentation curve for sample $Co_{77}Si_{11,5}B_{11,5}$ after heat treatment

The ultimate tensile strength test (UTS) was carried out on the Zwick/Z100 testing machine. The results were processed using the Test X Pert Master computer software integrated with the Zwick/Z100 testing machine.

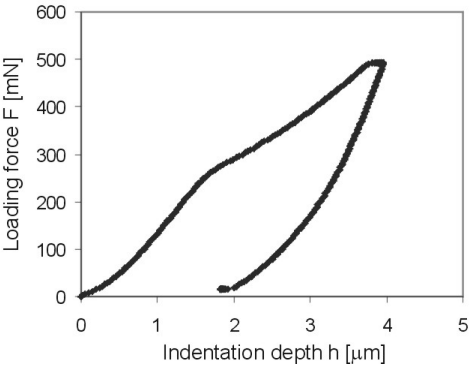

Fig. 4. Irregular indentation curve for sample $Co_{68}Fe_4Mo_1Si_{13,5}B_{13,5}$ after heat treatment

Table 1.
Chemical composition, state and number of indents investigated alloys

nr	Alloy	State	Number of all indents	Number of regular indents
1	$Co_{77}Si_{11,5}B_{11,5}$	amorphous	10	6
2	$Co_{77}Si_{11,5}B_{11,5}$	400°C/1h	10	9
3	$Co_{68}Fe_4Mo_1Si_{13,5}B_{13,5}$	amorphous	10	8
4	$Co_{68}Fe_4Mo_1Si_{13,5}B_{13,5}$	400°C/1h	10	8
5	$Fe_{78}Si_{13}B_9$	amorphous	20	8
6	$Fe_{78}Si_{13}B_9$	400°C/1h	10	9

3. Results and discussion

3.1. Martens hardness

Depth sensing indentation technique DSI was used for determining of local mechanical properties on 3 different materials in amorphous state and annealing in 400°C per 1 hour in argon atmosphere (Fig. 5).

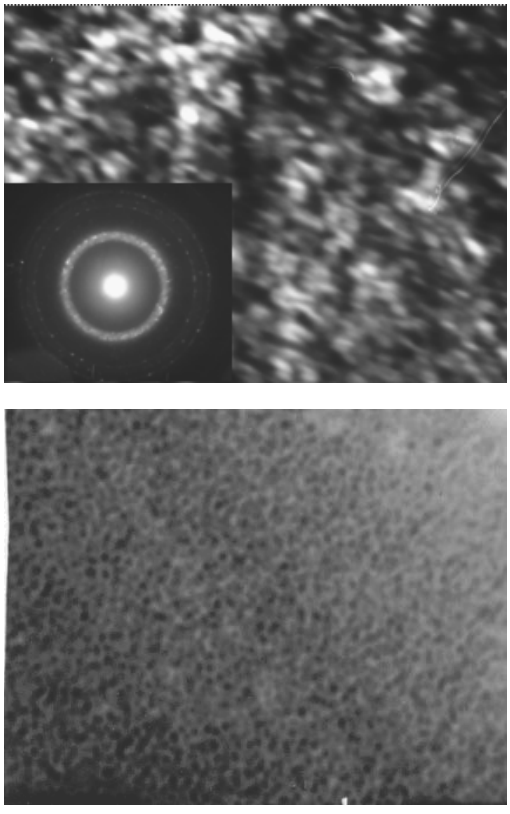

Fig. 5. Structure of the metallic ribbons obtained in melt spinning technique after heat treatment in temperature 400°C/1h a) $Co_{77}Si_{11,5}B_{11,5}$, b) $Co_{68}Fe_4Mo_1Si_{13,5}B_{13,5}$

The measured hardness values are scattered in a wide range - from HM=595 up to HM=5259 (Table 2). The corresponding range of the „classic“ Vickers hardness values is: for HM=595÷5259 MPa is HV=125÷1105.

Table 2.
Scatter and mean values of Martens hardness HM [MPa]

Alloy	state	HM	Standard deviation
$Co_{77}Si_{11,5}B_{11,5}$	amorphous	2281	1112
	400°C/1h	3269	921
$Co_{68}Fe_4Mo_1Si_{13,5}B_{13,5}$	amorphous	2573	737
	400°C/1h	2668	927
$Fe_{78}Si_{13}B_9$	amorphous	2085	862
	400°C/1h	2524	1036

The observed irregularity of the indentation curve was due to unusual shape of metallic ribbon (cross section was very thin and his area was a little uneven) and caused by lowered stiffness of the contact sample - indenter. No cracking, fracturing or similar ribbon damage was observed.

The big standard deviation values and the irregular F-h curves obtained from the micro-hardness tests (Fig. 4) may be caused by bending of the mounted ribbon under the indenter load and by the unevenness of the side surface, whose state results from the fabrication process - melt spinning.

According [1], there is a relation between the “classic” Vickers hardness HV and indentation H_{IT}: HV=0,0945 H_{IT}. H_{IT} is indentation hardness respecting elastic unloading of the indent.

3.2. Indentation modulus E_{IT}

The unloading part of indentation curve, responsible for modulus determination, is extremely sensitive to the contact stiffness between the indenter and the tested sample. All measured values are affected by this effect. Small effect means higher value of E_{IT}, therefore the max. values of E_{IT} see on Fig. 6.Taking this into account, one can conclude that all measured values of E_{IT} can be used for the comparison of materials, influence of heat treatment, etc.

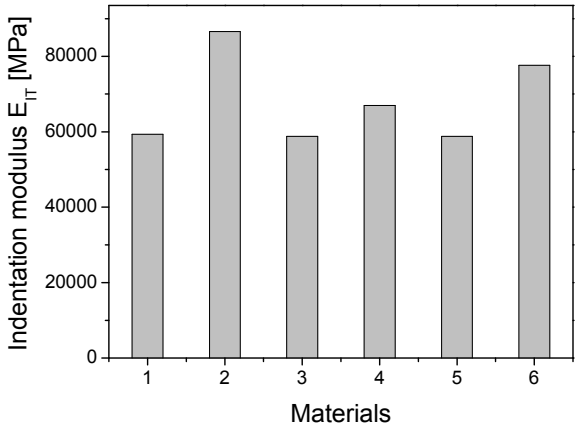

Fig. 6. Maximum values of indentation modulus E_{IT}

It follows clearly from this Table that E_{IT} values for the heat-treated materials are higher (46 % – material 2/1, 14 % – material 4/3, 32 % – material 6/5, see also Table 5) than that for the amorphous states. This conclusion corresponds well to the fact, that Young's modulus of amorphous materials is 60-80% of the Young's modulus of polycrystalline material, due to higher order in a crystal.

Respecting the number and scatter of the test values one can state that there are no significant differences in E_{IT} values between materials $Co_{77}Si_{11,5}B_{11,5}$, $Co_{68}Fe_4Mo_1Si_{13,5}B_{13,5}$, $Fe_{78}Si_{13}B_9$ in amorphous state/heat treated state, mainly in the amorphous state (Fig. 6).

The average of Martens hardness and large value of deviation standard from considerable dispersion of results of measurement, can't be explained as the fluctuations of chemical composition of metallic ribbons.

3.3. Work for deformation

The measured energy values W as well the hardness values HM are also affected by „sample stiffness"; however both, W and HM, are influenced much less than in case of E_{IT}. The effect of stiffness on H and W is opposite to the stiffness effect on E_{IT}. It means that the most probable values of energy are the minimum measured values; in case of hardness the most probable values are the maximum values. The minimum values of indentation energy are in Table 3.

Based on minimum energy, both W_{total} and W_{plast} are lower for heat-treated states $Co_{77}Si_{11,5}B_{11,5}$ (Fig. 6, 7), $Co_{68}Fe_4Mo_1Si_{13,5}B_{13,5}$ (Figs. 8, 9), $Fe_{78}Si_{13}B_9$ (Figs. 10, 11) than that for amorphous, while W_{elast} is lower in heat-treated state only formaterial $Co_{77}Si_{11,5}B_{11,5}$ and $Fe_{78}Si_{13}B_9$. Alloy $Co_{68}Fe_4Mo_1Si_{13,5}B_{13,5}$ exhibits smaller changes due to heat treatment, based on both mean and minimum values analysis, if compare with $Co_{77}Si_{11,5}B_{11,5}$ and $Fe_{78}Si_{13}B_9$ alloys.

For all materials, both at the amorphous state and after the heat treatment, most of the total energy used for deformation (indenter's penetration) is the elastic strain energy (Figs. 7-12).

In amorphous state the average values of W_{total}, W_{plast}, and W_{elast} are close to the ternary alloys $Co_{77}Si_{11,5}B_{11,5}$ the and $Fe_{78}Si_{13}B_9$ however for alloy $Co_{68}Fe_4Mo_1Si_{13,5}B_{13,5}$ are lower for ca. 20-25%. In case of heat-treated alloys the lowest average value of W_{total}, W_{plast}, and W_{elast} characterize the alloy $Co_{77}Si_{11,5}B_{11,5}$ and the highest ones the alloy $Fe_{78}Si_{13}B_9$.

All measured values do not differ significantly between the investigated materials, as well as comparing the amorphous state versus the heat-treated one. It is important that the ratio of elastic energy/total energy (52-58 %) is higher than that for plastic energy/total energy (42-48 %).

Ratio of elastic and total indentation energy $\eta_{IT} = W_{elast}/W_{total}$ was calculated on two ways: (i) based on mean values - η_{IT} (mean) and, respecting the stiffness effect also (ii) based on minimum values - η_{IT} (min) reflecting their higher probability (Table 4).

Table 3.
Mean and minimum values of indentation energy in 10^{-7} J

Alloy	State	Mean values of indentation energy			Minimum values of indentation energy		
		W_{total}	W_{elast}	W_{plast}	W_{total}	W_{elast}	W_{plast}
$Co_{77}Si_{11.5}B_{11.5}$	amorphous	7.73	4.35	3.38	4.46	2.39	2.07
	400°C/1h	5.35	2.93	2.42	3.82	1.97	1.85
$Co_{68}Fe_4Mo_1Si_{13.5}B_{13.5}$	amorphous	5.98	3.22	2.76	4.58	2.33	2.20
	400°C/1h	6.19	3.62	2.57	4.24	2.34	1.78
$Fe_{79}Si_{13}B_9$	amorphous	7.56	4.46	3.10	4.35	2.51	1.85
	400°C/1h	7.13	4.28	2.85	4.02	1.93	1.99

Table 4.
Ratio of elastic and total indentation energy $\eta_{IT} = W_{elast} / W_{total}$

Alloy	State	Ratio of elastic and total indentation energy η_{IT}	
		η (mean) [%]	η (min) [%]
$Co_{77}Si_{11.5}B_{11.5}$	amorphous	55.3	53.5
$Co_{68}Fe_4Mo_1Si_{13.5}B_{13.5}$	amorphous	54.3	50.9
$Fe_{79}Si_{13}B_9$	amorphous	59.8	57.6
Mean		56.4	54.0
$Co_{77}Si_{11.5}B_{11.5}$	400°C/1h	54.2	51.5
$Co_{68}Fe_4Mo_1Si_{13.5}B_{13.5}$	400°C/1h	59.2	55.2
$Fe_{79}Si_{13}B_9$	400°C/1h	59.3	48.1
Mean		57.5	51.6

Table 5.
Influence of heat treatment on local mechanical properties

Mat.	HM	HM_{max}	E_{max}	$W_{total\ min}$	$W_{elast\ min}$	W_{plast}
2/1	1.71	1.40	1.46	0.86	0.83	0.89
4/3	1.02	1.19	1.14	0.92	1.00	0.81
6/5	2.47	1.17	1.32	0.92	0.77	1.08

The relation between W_{elast} and W_{total} does not depend on the absolute value of total indentation energy, for all regular indentation curves (very low hardness or extremely high hardness). Therefore, it is not so sensitive to contact stiffness influence.

During deformation, the larger part of indentation energy is accumulated via elastic strain; the smaller part is transformed to the unrecoverable plastic strain. The elastic behaviour of all materials is extremely high, independent from material and its state (amorphous / heat-treated).

In Table 5 are factors they represent the influence of heat treatment on mechanical properties of individual materials. The factors are calculated for heat treated state/amorphous state.

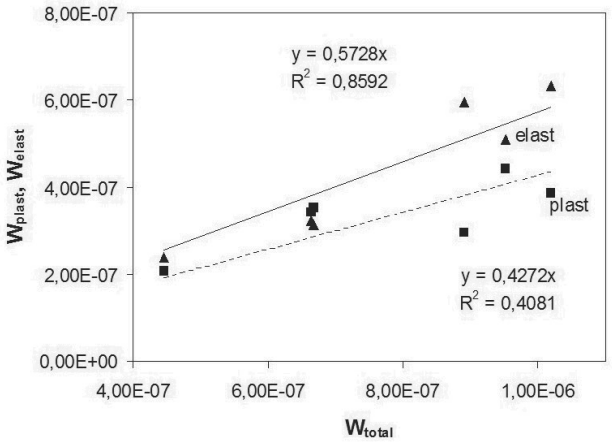

Fig. 7. Elastic reverse deformation work W_{elast} versus total mechanical work W_{total} for alloy $Co_{77}Si_{11,5}B_{11,5}$ in amorphous state

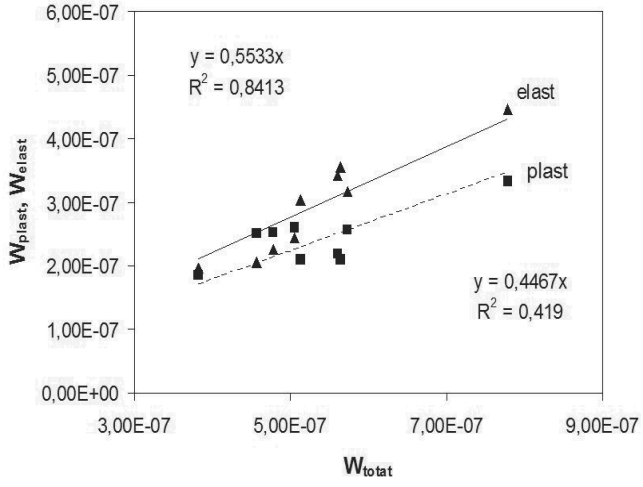

Fig. 8. Elastic reverse deformation work W_{elast} versus total mechanical work W_{total} for alloy $Co_{77}Si_{11,5}B_{11,5}$ after thermal annealing in 400°C/1h

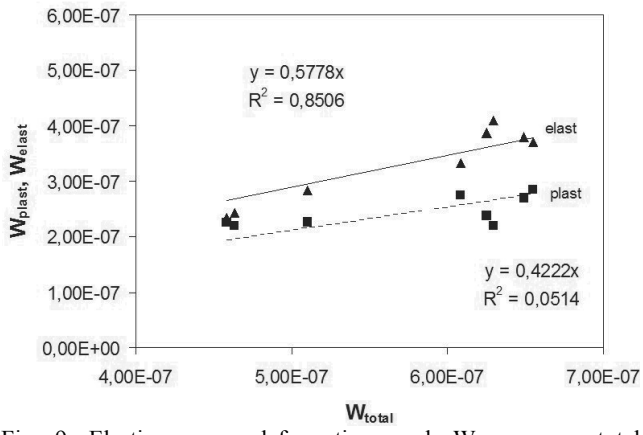

Fig. 9. Elastic reverse deformation work W_{elast} versus total mechanical work W_{total} for alloy $Co_{68}Fe_4Mo_1Si_{13,5}B_{13,5}$ in amorphous state

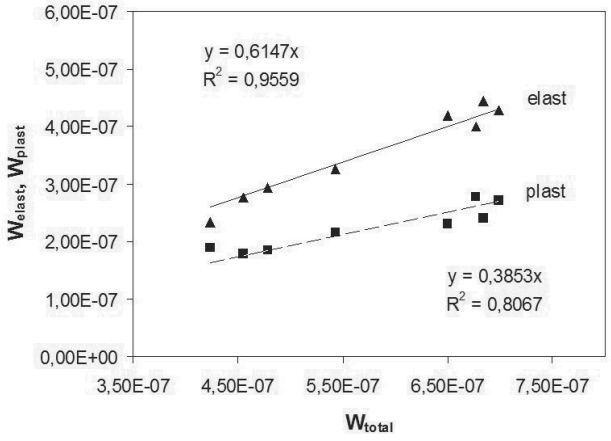

Fig. 10. Elastic reverse deformation work W_{elast} versus total mechanical work W_{total} for alloy $Co_{68}Fe_4Mo_1Si_{13,5}B_{13,5}$ after thermal annealing in 400°C/1h

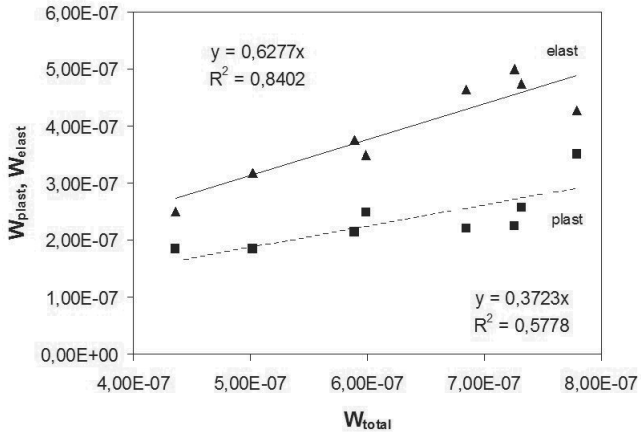

Fig. 11. Elastic reverse deformation work W_{elast} versus total mechanical work W_{total} for alloy $Fe_{79}Si_{13}B_9$ in amorphous state

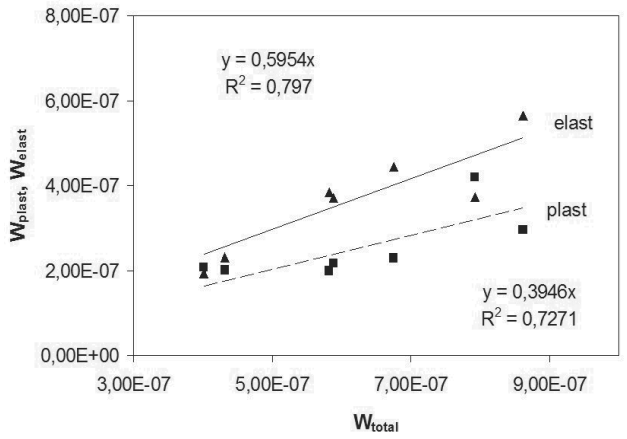

Fig. 12. Elastic reverse deformation work W_{elast} versus total mechanical work W_{total} for alloy $Fe_{79}Si_{13}B_9$ after thermal annealing in 400°C/1h

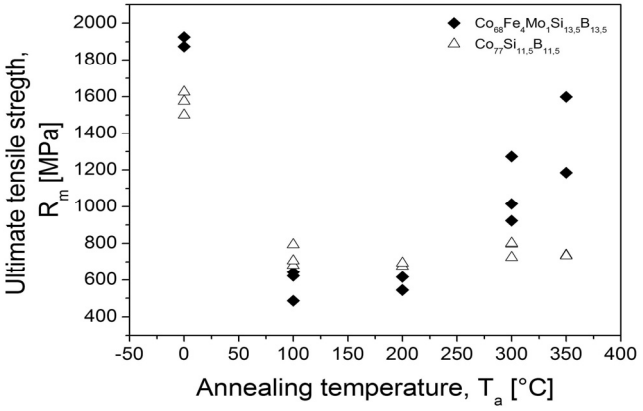

Fig. 13. Ultimate tensile strength UTS in the Co-base metallic ribbons

The mechanical properties tests indicate that the metallic ribbons based on cobalt exhibit best ultimate tensile strength UTS in amorphous state. After annealing in temperature 100°C and 200°C per 1 hour UTS decrease a few times (Fig. 13). For ternary alloy UTS after annealing in temperature 300°C and 350°C is almost the same value but for multicomponent alloy is higher two times.

Investigations of metallic $Co_{68}Fe_4Mo_1Si_{13,5}B_{13,5}$ ribbon fracture in amorphous state after break in tensile test showed their ductile character with vein pattern morphology, typical for metallic amorphous materials of high strength and ductility (Fig. 14).

The fracture of failed metallic ribbon $Co_{68}Fe_4Mo_1Si_{13,5}B_{13,5}$ after isothermal annealing had smooth surfaces and such morphology signifies embrittlement of annealed alloy (Fig. 15).

4. Conclusions

No significant differences between both ternary ($Co_{77}Si_{11,5}B_{11,5}$, $Fe_{78}Si_{13}B_9$) alloys in local mechanical properties martens hardness (HM), indentation modulus (E_{IT}) and energy for the total indentation deformation (W) were observed for amorphous state but differences between ternary and multicomponent alloys were observed. In heat treated state small differences between materials were observed too.

Fig. 13. SEM image of the ductile fracture with vein pattern morphology of amorphous $Co_{68}Fe_4Mo_1Si_{13,5}B_{13,5}$ ribbon in as-quenched state

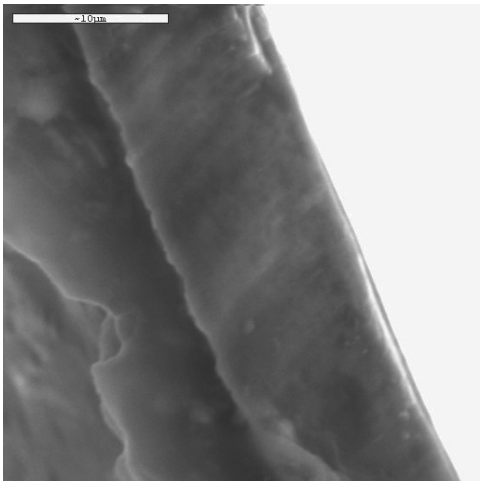

Fig. 14. SEM micrograph of brittle fracture surface of $Co_{68}Fe_4Mo_1Si_{13,5}B_{13,5}$ ribbon annealed in 300°C/1h

All materials in heat treated stage (2, 4, 6 Tabl. 1) has:

- higher Martens hardness (HM),
- higher indentation modulus (E_{IT}),
- lower energy for the total indentation deformation W_{total}, energy of elastic deformation W_{elast}, energy of plastic deformation W_{plast} except for ratio (amorphous/heat-treated) of plastic energy W_{plast} for alloy $Fe_{78}Si_{13}B_9$,

when compare with amorphous stage of the same kind of alloys.

Highest effect of influencing by heat treatment was observed for ternary alloys ($Co_{77}Si_{11,5}B_{11,5}$; $Fe_{78}Si_{13}B_9$) than for multicomponent alloy ($Co_{68}Fe_4Mo_1Si_{13,5}B_{13,5}$).

References

[1] J. Alcala, A.E. Giannakopoulos, S. Suresh, Continuous measurements of load-penetration curves with spherical micro-indenters and the estimation of mechanical properties, Journal of Materials Research 13 (1998) 1390-1395.

[2] M. Besterci, L. Pešek, P. Zubko, P. Hvizdos, Mechanical properties of phases in Al–Al_4C_3 mechanically alloyed material measured by depth sensing indentation technique, Materials Letters 59 (2005) 1971-1975.

[3] I.A. Figueroa, I. Betancourt, G. Lara, J. A. Verduzco, Effect of B, Si and Cr on the mechanical properties of Fe-based amorphous metallic ribbons', Journal of Non-Crystalline Solids 351 (2005) 3075-3080.

[4] A.R. Franco, G. Pintaude, A. Sinatora, C.E. Pinedo, A.P. Tschiptschin, The use of a Vickers indenter in depth sensing indentation for measuring elastic modulus and Vickers hardness, Materials Research 7/3 (2004) 4-9.

[5] M. Gögebakan, Mechanical properties of AlYNi amorphous alloys, Journal of Light Metals 2 (2002) 271.

[6] W.H. Jiang, F.X. Liu, Y.D.Wang, H.F. Zhang, H. Choo, P.K. Liaw, Comparison of mechanical behavior between bulk and ribbon Cu-based metallic glasses, Materials Science and Engineering 430 (2006) 350-354.

[7] J. Konieczny, L.A. Dobrzański, L. Pešek, Mechanical properties of metallic ribbons based on cobalt by depth sensing indentation technique, Proceedings of 11th International Scientific Conference on Contemporary Achievements in Mechanics, Manufacturing and Materials Science, Gliwice-Zakopane, 2005, 492-496. CD-ROM.

[8] J. Konieczny, L. A. Dobrzanski, A. Przybyl, J. J. Wyslocki Structure and magnetic properties of powder soft magnetic materials, Journal of Achievements in Materials and Manufacturing Engineering 20 (2007) 139-142.

[9] P. Kwapuliński, J. Rasek, Z. Stokłosa, G. Haneczok, Magnetic properties of amorphous and nanocrystalline alloys based on iron, Proceedings of 9th Jubilee Scientific International Conference, Achievements in Mechanical and Materials Engineering, Gliwice-Sopot-Zakopne, 2000, 341-344.

[10] P.L. Larsson, A.E. Giannakopoulos, E. Soderlund, D.J. Rowcliffe, R. Vestergaard, Analysis of Berkovich Indentation, International Journal of Solids and Structures 33/2, (1996) 221.

[11] S. Lesz, R. Nowosielski, A. Zajdel, B. Kostrubiec, Z. Stokłosa, Structure and magnetic properties of the amorphous $Co_{80}Si_9B_{11}$ alloy, Journal of Achievements in Materials and Manufacturing Engineering 18 (2006) 155-158.

[12] Y. Lu, P.K. Liaw, The Mechanical Properties of Nanostructured Materials, Journal of The Minerals, Metals and Materials Society 3 (2001) 31-32.

[13] D. G. Morris, Strength and ductility of nanocrystalline materials: What do we really understand?, Proceedings of 22nd Riso International Symposium on Materials Science, Roskilde, Denmark, 2001, 89-104.

[14] W.C. Oliver, G.M. Pharr, An improved technique for determining hardness and elastic modulus using load and displacement sensing indentation experiments, Journal of Materials Research 7 (1992) 721-726.

[15] W.C. Oliver, G.M. Pharr, Measurement of hardness and elastic modulus by instrumented indentation: Advances in understanding and refinements to methodology, Journal of Materials Research 19/1 (2004) 3-20.

[16] L. Pešek, L.A. Dobrzański, P. Zubko, J. Konieczny, Mechanical properties of metallic ribbons investigated by depth sensing indentation technique, Journal of Magnetism and Magnetic Materials 304 (2006) 645-e647.

[17] G.M. Pharr, W.C. Oliver, F. R. Brotzen, On the Generality of the Relationship between Contact Stiffness, Contact Area, and Elastic Modulus during Indentation, Journal of Materials Research 7 (1992) 613-617.

[18] T. Raszka, A. Przybył, Optimisation of soft magnetic properties in $Fe_{83-X}Co_XNb_3B_{13}Cu_1$ (x=10, 30, 40) amorphous alloys, Proceedings of 13th Jubilee Scientific International Conference, Achievements in Mechanical and Materials Engineering, AMME'2005, Gliwice-Wisła, 2005, 535-538.

[19] C.A. Schuh, T.G. Nieh, A survey of instrumented indentation studies on metallic glasses, Journal of Materials Research 19/1 (2004) 46-49.

[20] D. Szewieczek, A. Baron, Electrochemical corrosion and its influence on magnetic properties of $Fe_{75,5}Si_{13,5}B_9Nb_3Cu_1$ alloy, Proceedings of 13th Jubilee Scientific International Conference, Achievements in Mechanical and Materials Engineering, AMME'2005, Gliwice-Wisła, 2005, 631-634.

[21] D. Szewieczek, S. Lesz, Influence of structure on the evolution of magnetic and mechanical properties of amorphous and nanocrystalline $Fe_{85.4}Hf_{1.4}B_{13.2}$ alloy, Journal of Materials Processing Technology 162-163 (2005) 254-259.

[22] D. Szewieczek, J. Tyrlik-Held, S. Lesz, Changes of mechanical properties and fracture morphology of amorphous tapes involved by heat treatment, Journal of Materials Processing Technology 109 (2001) 190-195.

[23] ISO- 14577 - Metallic materials – Instrumented indentation test for hardness and materials parameters.